Progress in Physics of Applied Materials 3 (2023) 15–28

Semnan University

Progress in Physics of Applied Materials

journal homepage: https://ppam.semnan.ac.ir/

Study of structure, morphology, optical absorption, and gap modulation of Activated carbon (AC) / NiO, Fe_3O_4, and Co_3O_4 oxide nanocomposites

A. Haghir Ebrahim Abadi, M. M. Bagheri-Mohagheghi*

School of Physics, Damghan University, Damghan, Iran.

ARTICLE INFO

Article history:
Received: 26 April 2023
Revised: 20 June 2023
Accepted: 24 June 2023

Keywords:
Activated carbon,
Porous structure,
Green synthesis,
Energy storage,
Carbon/ metal oxides,
Nanocomposites

ABSTRACT

In this paper, the synthesis and structural and optical properties of activated carbon /metal oxide nanocomposites have been studied for energy storage applications. Activated carbon / nickel oxide, activated carbon / iron oxide, and activated carbon / cobalt oxide nanocomposites were synthesized by green synthesis from carbonaceous waste and their structural and optical properties were investigated. The prepared nanocomposites were characterized by X-ray diffraction (XRD), UV-Vis optical absorption spectroscopy, Scanning Electron Microscopy (SEM), Transmission Electron Microscopy (TEM), and Fourier-transform infrared (FTIR) spectroscopy techniques. The XRD results of the activated carbon / metal oxide nanocomposites, in addition to the activated carbon background, show a polycrystalline phase corresponding to NiO, Fe_3O_4, and Co_3O_4 oxides. According to SEM images, a carbon porous background was observed in nanocomposites, which is filled with metal oxide nanoparticles and these nanoparticles present on its surface non-uniformly. The band gap results of nanocomposites showed the presence of two shoulders clearly indicating the presence of two components in the nanocomposite, i.e., activated carbon (3.62-4.65 eV) and metal oxide (3.0 eV- 4.25 eV). In FTIR analysis, in addition of the carbon-carbon bonds, specific peaks were observed in the range of k=400-700 cm^{-1}, indicating that AC/ metal oxide nanocomposites have been successfully synthesized.

1. Introduction

Activated carbon (AC) is a porous carbonaceous material with a highly developed surface area and rich surface groups, which are widely used in numerous applications, including adsorption, catalyst support, gas separation, energy storage, solvent recovery, decolorizing, supercapacitors, and as black electrodes. The good electrical conductivity, good chemical stability, lightness, and high compatibility with the various processes of the common season, provide the use of this material in these applications [1–4].

Activated carbon is the most widely used electrode materials due to their large surface area (> 1000 m^2/gr), low cost, and easy processability, but they suffer from poor energy storage capacity and inferior rate capability. Therefore, to increase the efficiency of this material, the addition of metal oxides or semiconductors is used [5].

A good way to synthesize activated carbon is to use natural wastes such as date kernel, almond and walnut skin powder and burning them at high temperatures for preparation of black carbon and then activating with some agents such as NaCl, and NaOH. The effective surface area of the obtained activated carbon can be modified using citric acid (CA) and hydrochloric acid (HCl) to attain a porous and active structure. Also, in order to increase the efficiency of adsorbent activated carbon and metal oxides, these two materials can be combined as nanocomposite. Therefore, both activated carbons and pseudocapacitive materials need to be developed for better supercapacitors performance. Recent developments of composite materials which integrate carbon-based materials with either metal oxides/hydroxides or conducting polymers have demonstrated improved capacitive performance and cycle life through the synergistic effect of both electrochemical

* Corresponding author.
E-mail address: ***bmohagheghi@du.ac.ir***

DOI: 10.22075/PPAM.2023.30469.1054

double-layer capacitors (EDLC) and pseudo capacitance mechanisms [6–12].

Various types of carbon nanostructures such as carbon nanotubes, carbon 60 (C_{60}) compounds, carbon nano strings, carbon nanofibers, and active porous carbon have been used for various purposes in nanotechnology. The synthesis of carbon nanocomposites and active carbon AC with metal elements such as Si, Ni, Fe, and other elements or metal oxides such as SiO_2, SnO_2, ZnO, MnO_2, TiO_2, etc., is done in different ways to achieve the different results and goals [13–18]. The results and objectives are determined according to the expected end use for the composites. These applications include the use of carbon nanocomposites in cases such as photocatalysts, solar cells, supercapacitors, fuel cells, and nanomembranes to remove some pollutants such as heavy metals and dyes from water, air filters, sensors, hydrogen and lithium-ion battery, biomass conversion, and many other applications [19-22].

Nowadays, the general type of nanocomposite embedded with organic/inorganic materials is a fast-growing area of research. Researchers have given a major effort to obtain the nanoscale structures of nano-composite materials via innovative synthetic approaches. The properties of nanocomposite materials depend not only on the properties of their individual parents but also on their morphology and interfacial characteristics. Many types of carbon nanocomposites are used in several fields like ionic adsorption, batteries, etc. The magnetic oxide nanoparticles such as Fe_2O_3, MnO_2, NiO, and Co_2O_3 have plenty of applications in various fields such as environmental, catalysis, batteries, sensors, magnetic storage media, and contrast agents in magnetic resonance imaging [20-23]. Recently, Electrochemical Energy storage devices (EESD) with high energy density and power density, high optimized cycle life, economically viable, and eco-friendliness have attracted the attention of many researchers in the world [24]. Mainly, carbon-derived materials and their nanocomposites are used as the cathode, and a metal or metal oxide electrode serves as an anode. Metal electrodes have a high intrinsic volumetric capacity and, thus, higher energy densities and cycling stability than those of normal supercapacitors [25-28].

In this paper, activated carbon / iron oxide, activated carbon / nickel oxide, and activated carbon / cobalt oxide nanocomposites were synthesized and their physical properties were studied by X-ray diffraction (XRD), optical UV-Vis spectroscopy, Scanning Electron Microscopy (SEM) and Fourier-transform infrared (FTIR) spectroscopy techniques. The innovation of this work is the use of cheap carbon waste materials and easy synthesis steps for magnetic oxides of Fe_2O_3, NiO, and Co_2O_3 for supercapacitor and electrode materials application in energy storage batteries. The details of the synthesis steps by drawing synthetic flowcharts completely provide comprehensive information for the readers.

2. Experimental

This study has been reported the synthesis of activated carbon/metal oxide nanocomposites, which includes the preparation of activated carbon by green synthesis and then its addition to metal oxide nanoparticles.

Four main steps performed in the synthesis of activated carbon/metal oxide:

1. Synthesis of black carbon and activated carbon (AC) from Date kernel powder.
2. Synthesis of activated carbon (AC) / Iron oxide (Fe_3O_4) nanocomposite.
3. Synthesis of activated carbon (AC) / Nickel oxide (NiO) nanocomposite.
4. Synthesis of activated carbon (AC) / Cobalt oxide (Co_3O_4) nanocomposite.

Then, the prepared nanocomposites were characterized by X-ray diffraction (XRD), optical UV-Vis spectroscopy and Scanning Electron Microscopy (SEM) and Fourier-transform infrared (FTIR) spectroscopy techniques, and their various physical properties were investigated and compared.

2.1 Preparation of the carbon black (CB) and activated carbon (AC)

The synthesis of activated carbon consists of two main steps (Fig 1):

1. Carbonization: preparation of Date kernel powder as a raw material and heat treatment to remove non-useful organic contaminants and synthesis of black carbon (BC).

2. Chemical activation: the use of HNO_3 acid or NaCl solution to prepare activated carbon (AC) under annealing in nitrogen gas (N_2) atmosphere. The reason for chemical activation is to attain higher efficiency and better quality of activated carbon to create porosity and broken carbon bonds.

The synthesis steps of preparation of activated carbon are as follows:

Step 1: Preparation of date kernels raw powder.

Some date kernels are prepared, washed well and dried in the sun for a few days. After cleaning, the date kernels are transferred into the milling chamber to get a very fine powder. Then pass them through a sieve to separate the coarse grains.

Step 2: Preparation of carbon black.

Weigh 20 g of date kernel fine powder by a digital scale with precision 0.001 g. Putting date kernel powder inside the ceramic dishes and heat treatment in oven at T= 600 °C for 2 h under directing water vapor and nitrogen (N_2) or argon gas (Ar) and preparation of carbon black (CB).

Then, adding it to 150 cc distillated water and then mixing the resulting solution using a magnetic stirrer.

Step 3: Adding of the nitric acid (HNO_3) or NaCl as activating agent.

Adding the obtained black carbon powder (10 g) to the solution of distilled water (50 cc) and nitric acid (20 cc) while stirring with a magnetic stirrer. If NaCl is used for activation, we use 3 g for any 10 g of black carbon powder in 20 cc distilled water.

Step 4: Refluxing and heating.

Refluxing of the solution is carried out in an oil bath for 90 minutes at a temperature of T= 80 °C.

Then, the resulting gel is heated indirectly in an oil bath at T=100° C for 90 minutes.

Step 5: Preparation of activated carbon

The gel is dried by directly heating on the heater for 90 minutes at T=200 °C, and then grinding the resulting activated carbon powder.

In this step of the experiment, the activated carbon obtained from the previous step must be combined with metal oxide nanoparticles to obtain the nanocomposite. Thus, the activated carbon used for synthesis of nanocomposites with NiO, Fe_3O_4, and CO_3O_4.

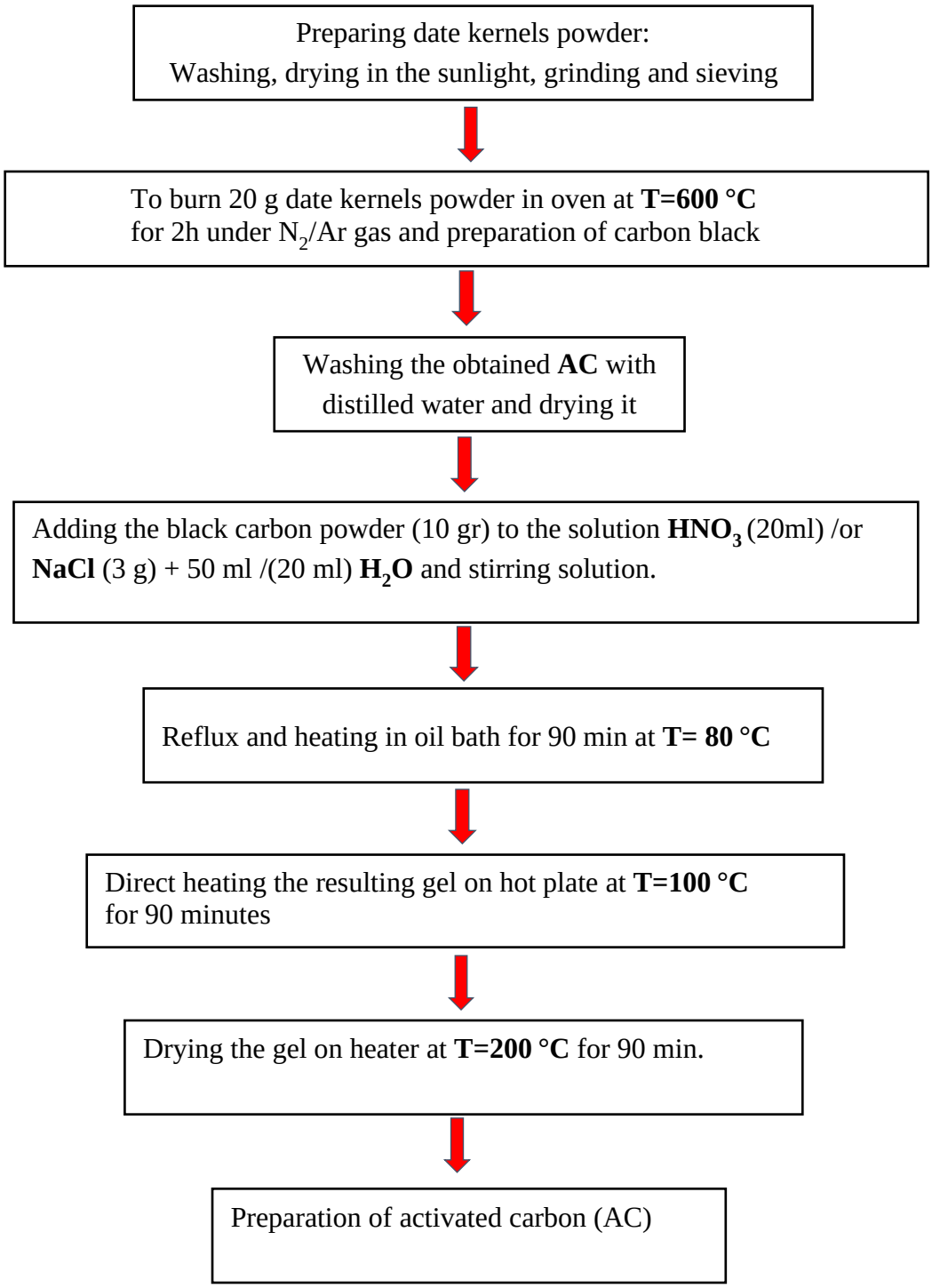

Fig. 1. Flowchart of synthesis of activated carbon using the NaCl and HNO_3 as activation agents.

2.2 Synthesis of activated carbon / (nickel oxide), (iron oxide), (cobalt oxide)

The amounts and materials required for the synthesis of activated carbon / metallic oxide nanocomposites are given in Table 1. The details of synthesis steps of activated carbon / nickel oxide, iron oxide and cobalt oxide nanocomposites are shown in Figure 2.

AC/NiO nanocomposite: Stirring for 15 minutes of $NiCl_2.6H_2O$ +H_2O

AC/ Fe_3O_4 nano composite: Stirring for 15 minutes of $FeCl_2$. $4H_2O$ + $FeCl_3.6H_2O$ + H_2O

AC/ Co_3O_4 nano composite: Stirring for 15 minutes of $CoCl_2.6H_2O$ +H_2O

-Adding ammonia / Oxalic acid to the solution as droplet.
-Adding activated carbon powder to the above solution and stirrer for 1 h.
-The solution is filtered and washed it with distilled water and alcohol.
-Dry the sample at T= 50°C for 12 h and annealing in air/Ar at T=450°C/ 200°C for 2h/6h
→ **AC/NiO nanocomposite.**

-Adding ammonia to the solution as droplet.
-Adding activated carbon powder to the above solution and stirrer for 1 h.
-Wash the brown precipitate formed with distilled water and alcohol.
-Dry the sediment at T= 80°C for 10 h and annealing in air T=200°C for 4 h.
→ **AC/Fe_3O_4 nanocomposite.**

-Adding ammonia to the solution as droplet.
-Adding activated carbon powder to the above solution and stirrer for 1 h.
-The solution is filtered and washed it with distilled water and alcohol.
-Drying the green powder at T= 50°C for 12 h and annealing in air T=200°C for 4 h.
AC/ Co_3O_4 nanocomposite

Fig. 2. Stages of green synthesis of activated carbon (AC) /NiO, Fe_2O_3 and Co_3O_4. nanocomposites.

Table 1. Raw materials for the synthesis of activated carbon/metallic oxide.

Material for AC/NiO	Weight	**Material for AC/Fe_3O_4**	Weight	**Material for AC/CO_3O_4**	Weight
activated carbon	0.5 g	activated carbon	0.75 g	Activated carbon	0.5 g
$NiCl_2.6H_2O$		**$FeCl_2.4H_2O$**	1.48 g + 4 g	**$CoCl_2.6H_2O$**	4.75 g
Method 1:	4.75 g	**$FeCl_3.6H_2O$**			
Method 2:	4.92 g				
Method 1: **Ammonium**	10 ml				
Method 2: **Oxalic acid**	3.78 g	**Ammonium** (NH_3)	40 ml	**Ammonium** (NH_3)	10 ml
Method 1: **Distilled water**	100 ml				
Method 2: **Ethanol**	40 ml	Distilled water	120 ml	Distilled water	100 ml

3. Results and discussion

3.1. Structural properties

The X-ray diffraction pattern of activated carbon (AC) with NaCl and nitric acid (HNO_3) as activated agent and activated carbon nanocomposites with iron oxide, nickel oxide, and cobalt oxide are shown in Figure 3 and Figure 4. Figures 3(a) and 3(b) show the comparison of X-ray diffraction (AC) patterns of activated carbon with NaCl and HNO_3 which have two wide peaks, one with a strong background at $2\theta \approx 24^{\circ}$ corresponding to the (002) plane and wide peak of (100) plane due to natural amorphous carbon. As seen, background of X-ray diffraction pattern of NaCl is more than that of HNO_3, related to increasing the amorphous phase.

Fig. 4(a)-(f) shows the XRD patterns of activated carbon nanocomposites with nickel oxide with ammonia 4(a, b), oxalic acid 4(c, d), iron oxide 4(e), and cobalt oxide 4(f). All structures have a polycrystalline structure with a strong background.

For AC/NiO nanocomposite with ammonia annealed under Argon (Ar) gas, the phases of nickel hydroxide Ni $(OH)_2$ and nickel oxide (NiO) are shown on activated carbon. In Figure 4 (a), nickel hydroxide with peaks 2θ=18.98, 33.15, 38.61, 52.23, 59.17, and 62.72 are displayed, refer to (001), (100), (101), (102), (110), and (111) planes. In general, Ni $(OH)_2$ is characterized by two types of polymorphs α-Ni $(OH)_2$ and β-Ni $(OH)_2$. β-Ni $(OH)_2$ is clearly defined by the peak 2θ = 19.2, but α-Ni $(OH)_2$ is difficult to determine due to its irregular structure, but must show a wide peak in the range 2θ =15° -20° . The annealing process in air affects the crystallinity. During annealing process, water hydrate is removed from room temperature to T=200° C and at higher temperatures (T=450° C) nickel hydroxide is converted to nickel oxide (NiO), as seen in Figure 4(b). In Figure 4(b), in addition to the background of activated carbon, nickel oxide is shown with peaks at 2θ=37.26, 43.29, and 62.89, which correspond to (111), (200) and (220) planes.

As seen in Figure 4 (c), for synthesized AC/NiO nanocomposite with oxalic acid and annealing in argon gas at T=200° C, in addition to the peaks of nickel oxide and amorphous carbon, two peaks of 2θ = 44.5-85.1 are observed, which correspond to (111) and (200) planes for the cubic structure is nickel (Ni) metal. With annealing at T= 450° C in air, the oxide reactions are complete, and only amorphous carbon and nickel oxide (NiO) are formed (Figure 4(d)). Indeed, the use of oxalic acid in comparison with ammonia causes the formation of nickel metal phase, which turns into nickel oxide by annealing in air.

In Figure 4 (e) for AC/Fe_3O4 nanocomposite with ammonia, in addition to the amorphous carbon peaks, it shows other peaks related to the fcc cubic structure of Fe_3O_4 in 2θ= 29.94°, 35.27°, 35.27°, 42.8°, 56.67°, 62.22°, which correspond to (220), (311), (400), (511) and (440) planes, respectively.

In Figure 4 (f) for AC/Co_3O4 nanocomposite with ammonia, as shown in addition to the presence of activated carbon several peaks at angles 2θ=18.96°, 31.22°, 36.78°, 38.48°, 44.73° ,59.25°, 65.11° which are respectively in (111), (220), (311), (222), (400), (511) and (440) planes are observed which correspond to the fcc phase of the Co_3O_4 spinel structure.

Comparison of XRD patterns of activated carbon /metal oxide nanocomposites show that, nickel oxide, iron oxide, and cobalt oxide nanocomposites were successfully synthesized by embedded nanoparticles into the activated carbon matrix.

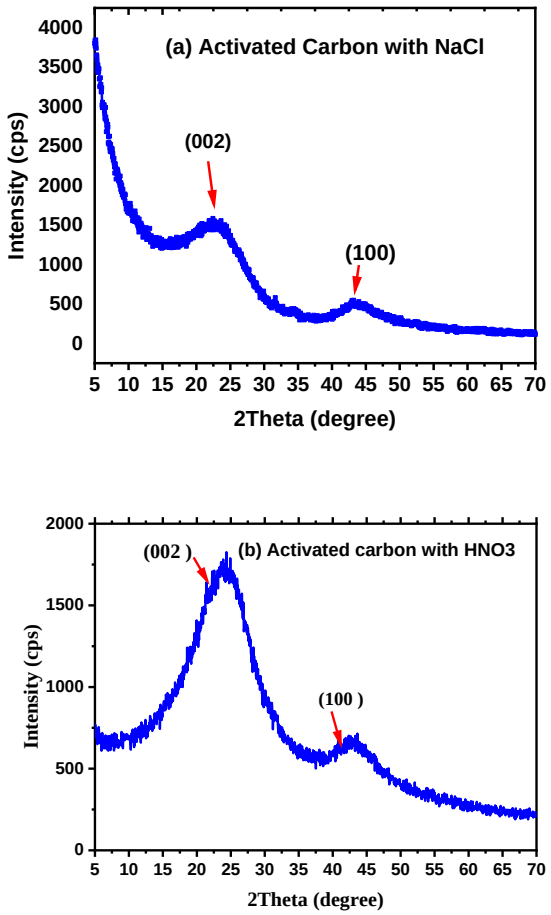

Fig. 3. The XRD patterns of (a) activated carbon with NaCl and (b) activated carbon with HNO_3.

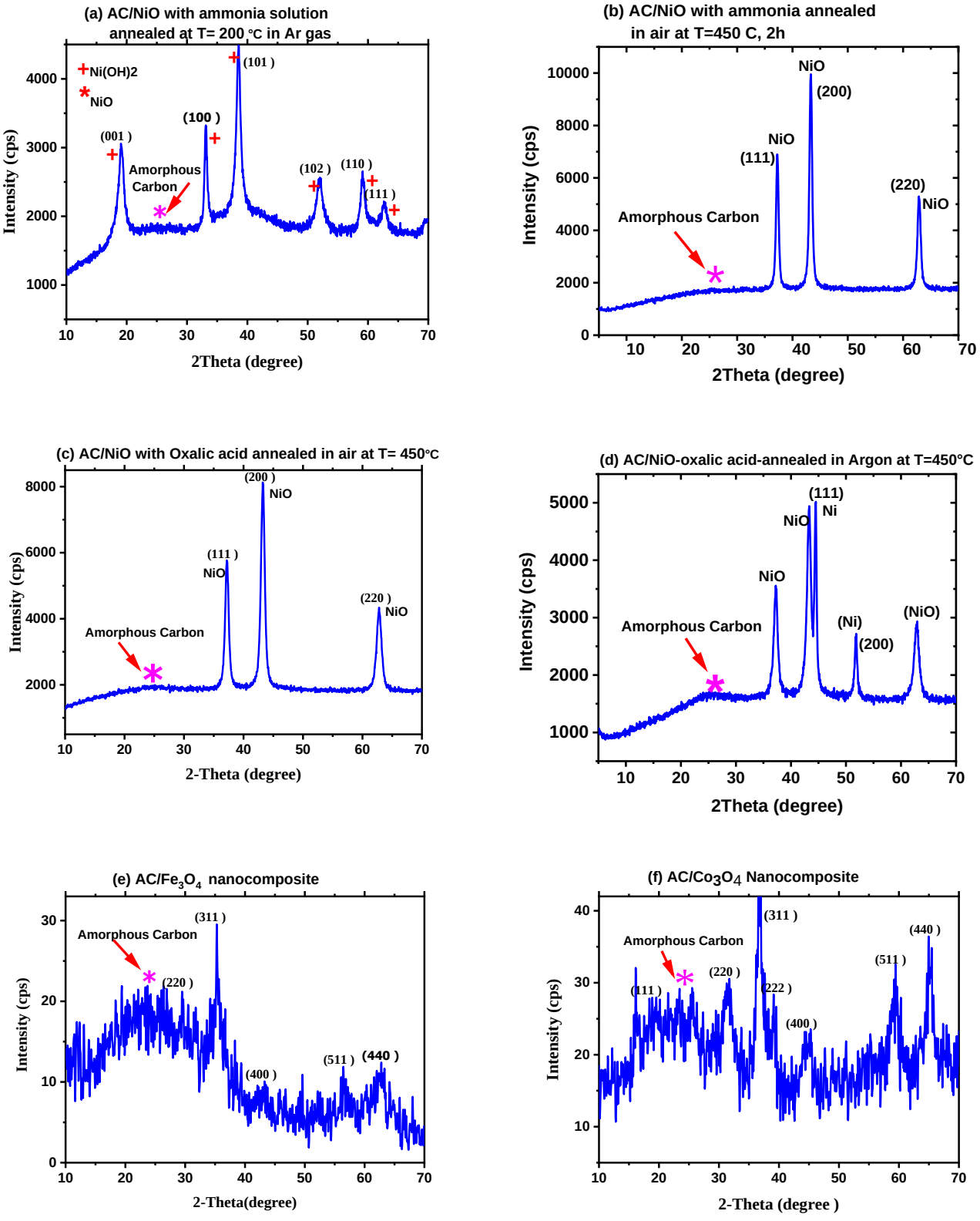

Fig. 4. The XRD patterns of nanocomposites (a) and (b) AC/NiO with Ammonia, (c) and (d) AC/NiO with oxalic acid, (e) AC/Fe_3O_4 and (f) AC/Co_3O_4.

3.2. Surface properties

3.2.1. Scanning Electron Microscope (SEM)

The SEM images of activated carbon (AC) and its nanocomposites with metal oxides of NiO, Fe_3O_4, and CO_3O_4 at different magnifications are shown in Figure 5 and Figure 6.

Figs. 5(a)-(c) show the presence of pores and porosity on activated carbon with nearly uniform distribution for both activation agents of NaCl and HNO_3. The difference between these two states of Figure 5(a) and Figure 5(b) is

in the morphology, so that for the NaCl state compared to the acid; the particles are coarser and the porosity seems to be more for HNO_3 acid. Indeed, due to chemical etching of HNO3, the porosity is increased.

The SEM images of AC/ oxides nanocomposites for NiO, Fe_3O_4 and CO_3O_4 are shown in Figure 6. It is seen that the metal oxide nanoparticles fill the pores of the activated carbon and are dispersed and unevenly distributed on its surface. The light phases represent metal oxide nanoparticles and the dark phases represent activated carbon. The morphology of AC/ NiO with ammonia (Figure 6 (a), (b)) is more plate-like and blade-like, but for AC/ NiO with oxalic acid (Figure 6 (c), (d)) it is granular-like and globule-like. The morphology of AC/ Fe_3O_4 (Figure 6 (e), (f)) and AC/CO_3O_4 (Figure (g), (h)) is granular-like and globule-like.

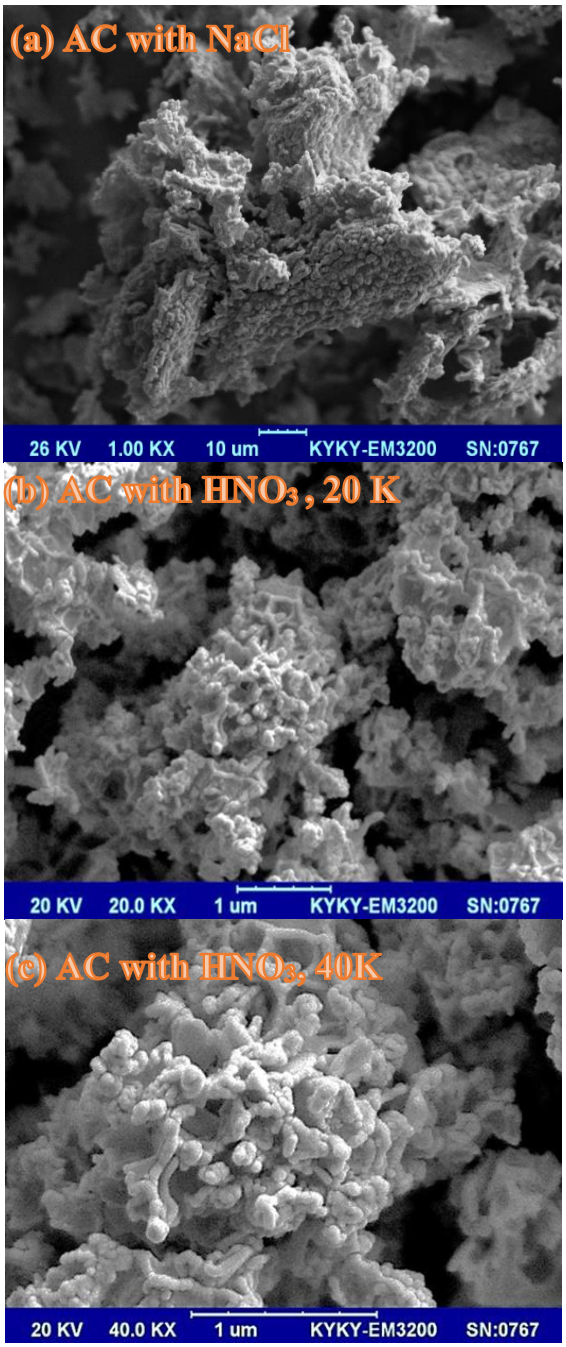

Fig. 5. The SEM images of (a) activated carbon with NaCl and activated carbon with HNO_3, (b) MAG: 20K, and (c) MAG:40K.

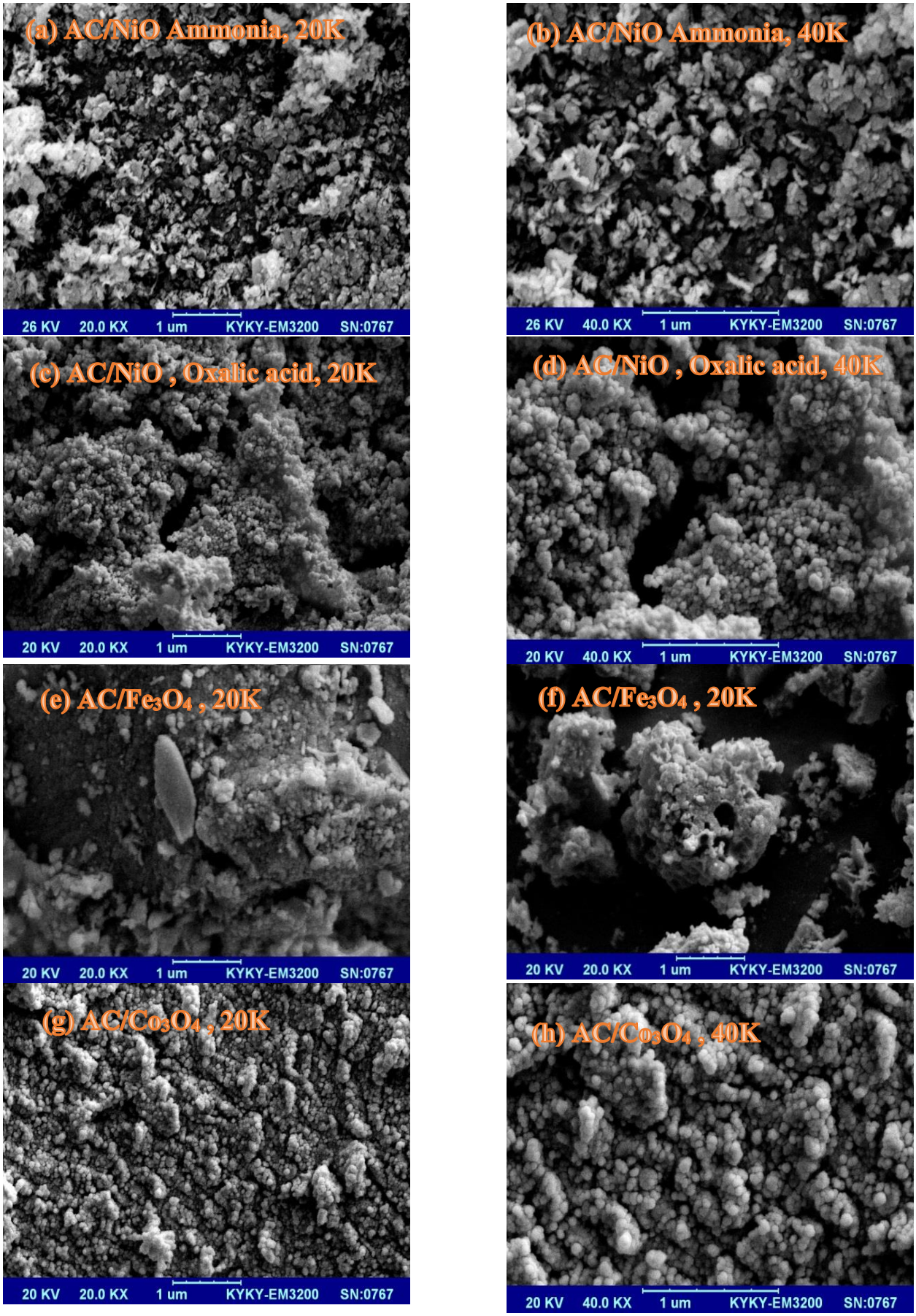

Fig. 6. SEM images of nanocomposites: (a), (b) AC / NiO with Ammonia, (c), (d) AC / NiO with Oxalic acid, (e), (f) AC/Fe_3O_4, and (g) , (h) AC/ Co_3O_4 .

3.2.2. Transmission electron microscope (TEM)

The TEM images of modified activated carbon (AC) and activated carbon/nickel oxide (AC/NiO) nanocomposites prepared at different magnifications are shown in Figure 7 (a) – (d). For activated carbon nanostructure (Figure 7(a) and (b)), the size and morphology of the particles are found almost uniform (light background), except for more thickness of activated carbon layer (dark background). Figure 7(c) and (d) show dark spots in the image that correspond to that part of activated carbon filled with nickel oxide nanoparticles. In the images, due to the high absorption of active carbon, the phases are darker compared with to metal oxide nanoparticles. It is observed that the morphology of activated carbon has changed after the placement of nickel oxide nanoparticles on it.

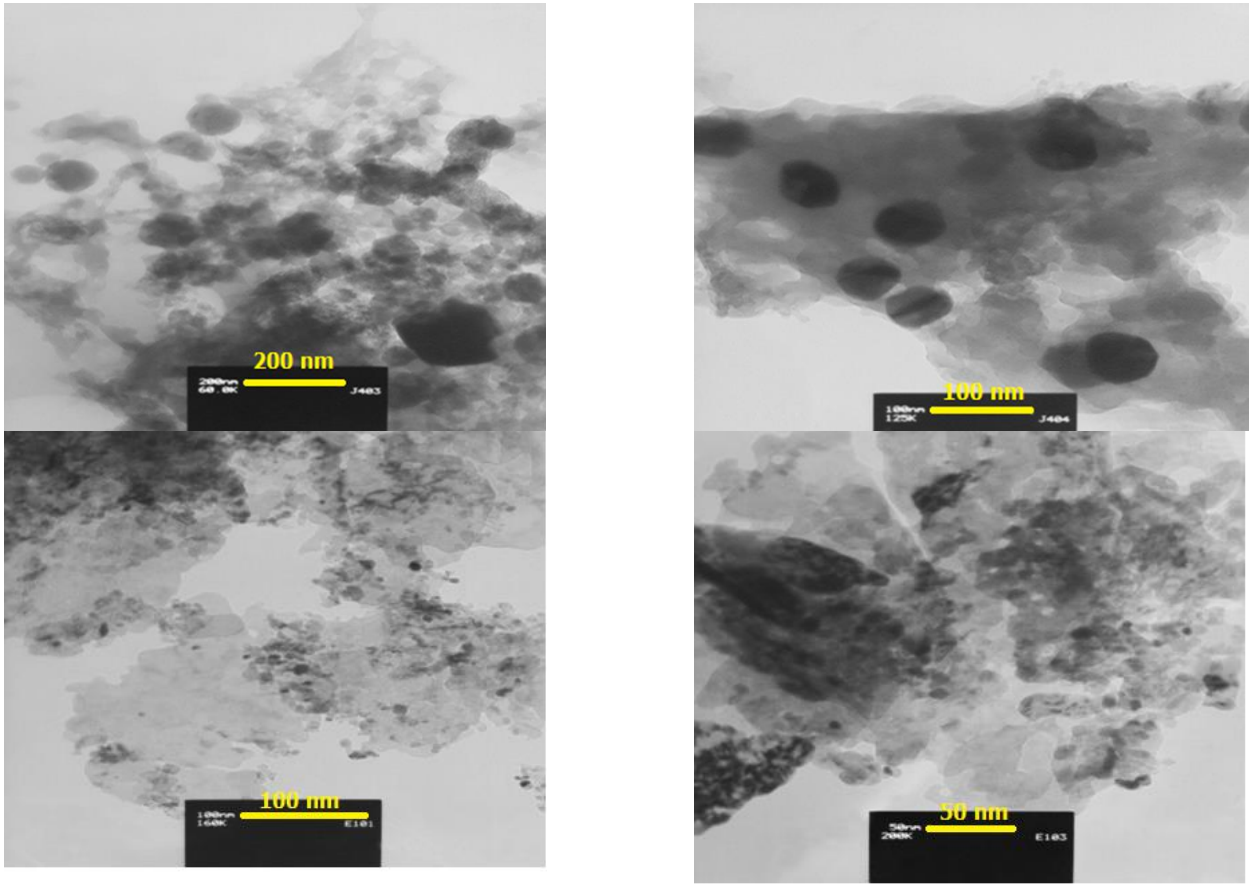

Fig. 7. TEM images for: (a) and (b) activated carbon, (c) and (d) AC/ NiO nanocomposites.

3.3. UV-Vis absorption analysis

3.3.1. Optical absorption coefficient (α)

The absorption coefficient (α) is obtained using the absorption spectrum (Equation 1) in the wavelength range of 190-1100 nm:

$$\alpha(\lambda) = 2.303\ A / d \quad (1)$$

Where A is the optical absorption and d is the nanoparticle size (~ 50 nm) in nanometers.

At first, for optical spectroscopy and measuring the absorbance (A) of the nanoparticles, the activated carbon / metal oxide composite powder was completely fine and 100 mg of it was dispersed in 5 cc of alcohol for 10 minutes by an ultrasonic device. Then 2 cc of the dispersed solution were poured in the spectrometer cell and the absorbance was measured according to the standard method.

In Figures 8(a)–(d), variation of the absorption coefficient (α) versus wavelength (λ) in nm for various AC/ metallic oxide nanocomposites are shown. As can be seen, the absorption edge is in the region of 260-400 nm, which tends to the shorter wavelength by adding a metal component.

As seen in Table 2 and Figure 8 (a): the activated carbon absorption peaks are at λ=300-350 nm, Figure 8 (b): AC / NiO nanocomposite absorption peaks are around λ=32-400 nm, in Figure 8 (c): AC / Fe_3O_4 nanocomposite absorption peaks are at λ=265-300 nm and in Figure 8 (d): AC / Co_3O_4 nanocomposite has absorption peaks at λ=280-350. Indeed, adsorption edge of nanocomposite in presence of oxide component, is shifted to shorter wavelength. This reduction is due to the presence of metal nanoparticles in the sample.

Table 2. The optical absorption and band gap of activated carbon and activated carbon / metal oxide nanocomposites.

Nanocomposite	Band gap Metal oxide	Band gap Activated carbon	Absorption edge range in UV (λ)
AC	-	3.60 eV	300-350 nm
AC/NiO	3.0 eV	3.85 eV	320-400 nm
AC/Fe_3O_4	4.25 eV	4.62 eV	265-300 nm
AC/Co_3O_4	3.65 eV	4.36 eV	280-350 nm

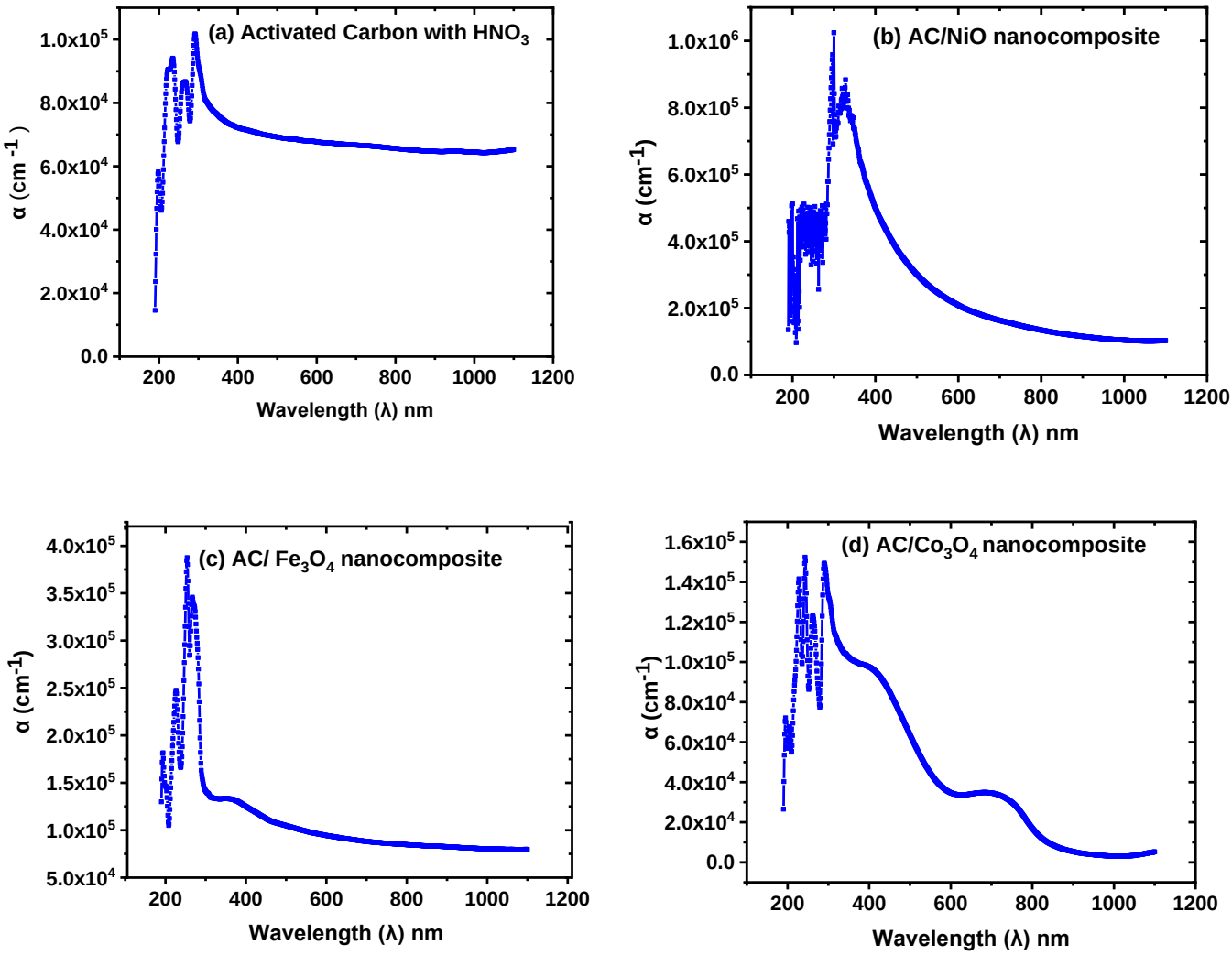

Fig. 8. The variation of the optical absorption coefficient (α) versus wavelength (λ): (a) activated carbon (AC) , (b) AC/NiO, (c) AC/Fe_3O_4, and (d) AC/Co_3O_4 nanocomposites.

3.3.2 Optical band gap of AC / MO nanocomposites

Using the Equation 2 by plotting $(\alpha h\nu)^2$ in terms of $(h\nu)$ (Tauc plot) and calculating the slope of the linear part of the curve, the bandgap value of the nanocomposite is obtained [29].

$$(\alpha h\upsilon)^2 = A\,(h\upsilon - E_g) \qquad (2)$$

Where α is the absorption coefficient, hυ is the energy of the incident photon; A is a numerical constant, and E_g is the band gap energy.

According to the diagrams in Figure 9, the band gap for nitric acid activated carbon powder is about 3.60 eV, for AC / NiO nanocomposite is about 3.0 eV (NiO), 3.85 eV (AC), for AC / Fe_3O_4 nanocomposite is about 4.25 eV (Fe_3O_4) 4.62 eV (AC), for nanocomposite AC / Co_3O_4 is about values of, 3.65 eV (Co_3O_4), and 4.36 eV (AC). As can be seen in the

band gap diagrams of nanocomposites, the presence of two shoulders clearly indicates the presence of two components in the nanocomposite, i.e., active carbon and metal oxide. Here, the difference in the energy gap for activated carbon in nanocomposites is due to the synthesis factors, including the growth process of nanoparticles, the amount of porosity, morphology, and the type of reducing agent, which is also mentioned in the others works [29-32]. In addition, as seen in Figure 10, the maximum increment in the energy gap is related to the composite with iron oxide, which is due to its inherent gap.

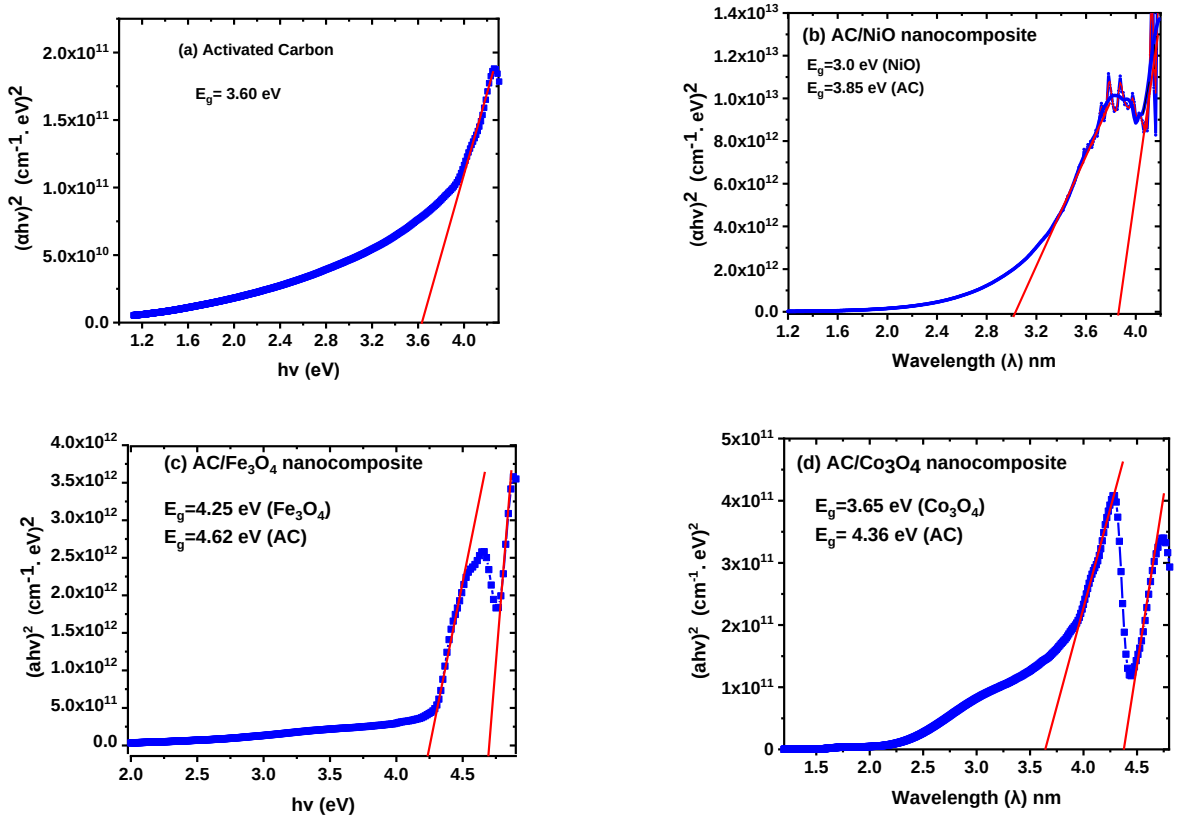

Fig. 9. The optical band gap of (a) activated carbon (AC), (b) AC/NiO, (c) AC/Fe_3O_4, and (d) AC/Co_3O_4 nanocomposites.

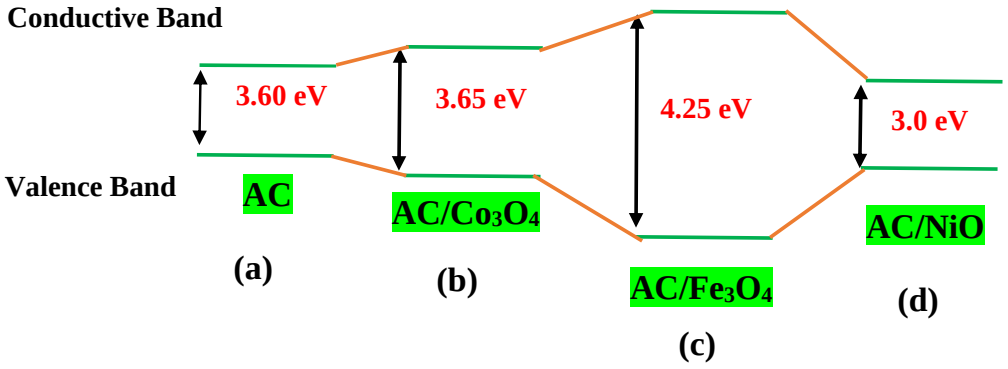

Fig. 10. The graphical view of optical band gap of (a) activated carbon (AC), (b) AC/ Co_3O_4, (c) AC/Fe_3O_4, and (d) AC/ NiO nanocomposites.

3.4. Infrared Fourier transform spectroscopy (FT-IR) analysis

For information on the presence of organic bonds and the type of bonds in activated carbon (AC) and activated carbon/metal oxide nanocomposites, the infrared optical transmission spectrum of powders in the range of k=400 cm^{-1} to 4000 cm^{-1} using FT-IR spectrophotometer, were obtained. Activated carbon and AC/MO nanocomposites FTIR patterns are shown in Figure 11 (a)-(d).

Activation of carbon with HNO_3 causes changes in the bond surface chemistry of the carbon. This method forms oxygenated surface groups and structures including N-O bonds (nitrate compounds and nitro group). Oxidation of

HNO_3 activated carbon may have similarities to aromatic hydrocarbons. Absorption peaks in the range of k=1600-1600 cm^{-1} can be due to the presence of oxygenated structures and structures containing N-O. The absorption peak in the range of k=1100-900 cm^{-1} also indicates that C-O bonded structures are affected. The absorption spectrum of nitric acid-activated carbon is shown in Figure 11(a). The main peaks include absorption peaks in k=1222 cm^{-1} and k=1385 cm^{-1} related to CO tensile vibrations, absorption peaks in k=1540 cm^{-1} related to dual tensile bond C = C, absorption peaks in k=2360 cm^{-1} related to triple bond C = CC, and the absorption peak at k=3410 cm^{-1} is related to OH tensile vibrations [29].

As can be seen in all patterns, there are specific peaks in the range of k=1570-1540 cm^{-1} and k=2370 cm^{-1} -2320 cm^{-1}, which are related to c-c bond vibrations and confirm that carbon is not lost during the synthesis of nanocomposites. There are also weak peaks in the range of k=3000 cm^{-1}-2800 cm^{-1}, which are related to C-H tensile vibrations. Peaks in the range of k=3600-3200 cm^{-1} are also related to the tensile vibrations of O-H water molecules [29, 30].

In addition to the vibrational bonds C-C and O-H, which were also present in the activated carbon, in Figure 11(b), the absorption peak at k=463 cm^{-1} can be attributed to the **Ni-O** bond [30] and the absorption peak at k=1617 cm^{-1} is related to the C = O tension. In Figure 11 (c), two other absorption peaks at k=445 cm^{-1} and k=638 cm^{-1} are observed, which are related to the vibrations of the **Fe-O** bond [31], and in Figure 11 (d) the absorption peaks at k=570 cm^{-1} and k=665 cm^{-1} are related to **Co-O** vibrations [32]. In Figure 11(b) and Figure 11(c), the absorption peak around k= 822 cm^{-1} can be attributed to the bending mode of aromatic compounds.

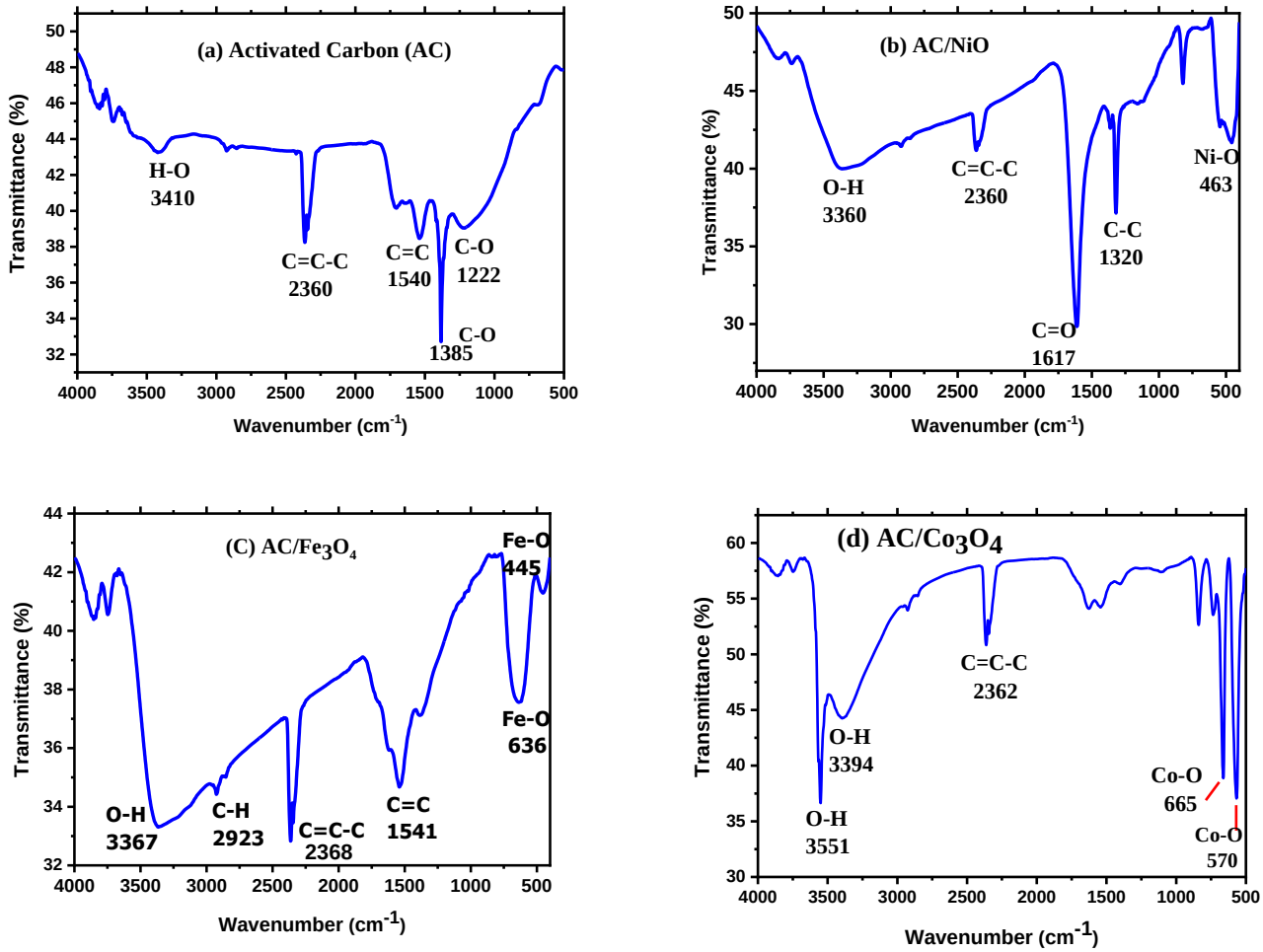

Fig. 11. FT-IR adsorption spectrum of activated carbon / metal oxide nanocomposites: (a) Activated Carbon (AC), (b) AC / NiO (C), (c) AC / Fe_3O4 , , and (d) AC / Co_3O_4.

4. Conclusion

In this work, activated carbon / nickel oxide, activated carbon / iron oxide, and activated carbon / cobalt oxide nanocomposites were prepared by green synthesis from carbonaceous waste and their structural and optical properties were investigated. The most important results obtained are:

(a) According to the XRD spectrum in the activated carbon sample with nitric acid-modified, two wide peaks are

observed at 2θ≈24° and 47° corresponding to the amorphous carbon. In nanocomposites, in addition to the activated carbon background, a polycrystalline phase corresponding to oxides of NiO, Fe3O4 and Co3O4 is observed. Intensity of peaks is increased with increasing the annealing temperature.

(b) According to SEM images of activated carbon and its nanocomposites with metal oxide, it is observed that activated carbon has fine holes and it is filled with metal oxide nanoparticles and these nanoparticles are present non-uniformly on its surface. Also, from the TEM images, a carbon dark background with nanoparticles is observed.

(c) The two shoulders observed in the band gap graph of nanocomposites clearly indicates the presence of two components, i.e., active carbon and metal oxide. The band gap for activated carbon powder, activated by nitric acid is about 3.62 eV, and with adding the metal oxide, the band gap of oxide component is in the rang of 3.0 eV-4.25 eV.

(d) According to the FTIR spectrum, functional groups can be observed in activated carbon modified with nitric acid and activated carbon metal oxide nanocomposites. The pattern show that carbon is not lost during synthesis. Specific peaks can also be seen in the range of k=400-700 cm-1, indicating that metal nanoparticles have been successfully synthesized.

References

[1] H. Hadoun, Z. Sadaoui, N. Souami, D. Sahel, and I. Toumert. "Characterization of mesoporous carbon prepared from date stems by H3PO4 chemical activation." Applied Surface Science 280 (2013) 1-7.

[2] J. Yongbin, T. Li, L. Zhu, X. Wang, and Q. Lin. "Preparation of activated carbons by microwave heating KOH activation." Applied surface science 254 (2007) 506-512.

[3] Y. Sait, and D. Yıldız. "Preparation and characterization of activated carbons from Paulownia wood by chemical activation with H3PO4." Journal of the Taiwan Institute of Chemical Engineers 53 (2015) 122-131.

[4] B. Corcho-Corral, M. Olivares-Marín, C. Fernández-González, V. Gómez-Serrano, and A. Macías-García. "Preparation and textural characterization of activated carbon from vine shoots (Vitis vinifera) by H3PO4—chemical activation." Applied Surface Science 252 (2006) 5961-5966.

[5] B. Saswata, T. Kuila, A. Kumar Mishra, R. Rajasekar, N. Hoon Kim, and J. Hee Lee. "Carbon-based nanostructured materials and their composites as supercapacitor electrodes." Journal of Materials Chemistry 22 (2012) 767-784.

[6] M. Ho, Y. P. S. Khiew, D. Isa, T. K. Tan, W. S. Chiu, and C. H. Chia. "A review of metal oxide composite electrode materials for electrochemical capacitors." Nano 9 (2014) 1430002.

[7] L.S. Zhong, J.S. Hu, H.P. Liang, A.M. Cao, W.G. Song, and L.J. Wan. "Self-Assembled 3D flowerlike iron oxide nanostructures and their application in water treatment." Advanced materials 18 (2006) 2426-2431.

[8] G. Jingming, and X. Lin. "Facilitated electron transfer of hemoglobin embedded in nanosized Fe3O4 matrix based on paraffin impregnated graphite electrode and electrochemical catalysis for trichloroacetic acid." Microchemical journal 75 (2003) 51-57.

[9] C. Z. Min, L.Y. Jiang, W. G. Song, and Y.G. Guo. "High-yield gas− liquid interfacial synthesis of highly dispersed Fe3O4 nanocrystals and their application in lithium-ion batteries." Chemistry of Materials 21 (2009) 1162-1166.

[10] K. Dong-Jun, Y. K. Lyu, H. N. Choi, I. H. Min, and W.Y. Lee. "Nafion-stabilized magnetic nanoparticles (Fe 3 O 4) for [Ru (bpy) 3] 2+ (bpy= bipyridine) electrogenerated chemiluminescence sensor." Chemical Communications 23 (2005) 2966-2968.

[11] T. J. Daou, J. M. Grenèche, G. Pourroy, S. Buathong, A. Derory, C. Ulhaq-Bouillet, B. Donnio, D. Guillon, and S. Begin-Colin. "Coupling agent effect on magnetic properties of functionalized magnetite-based nanoparticles." Chemistry of Materials 20 (2008) 5869-5875.

[12] S. Manfred, S. Olejnik, E. L. Salabas, W.Schmidt, and F. Schüth. "Scalable synthesis of activated carbon with superparamagnetic properties." Chemical communications 38 (2006) 3987-3989.

[13] S. Samik, P. Maji, D. A. Pethsangave, A. Roy, A. Ray, S. Some, and S. Das. "Effect of morphological ordering on the electrochemical performance of MnO2-Graphene oxide composite." Electrochimica Acta 317 (2019) 199-210.

[14] T. Xiaoqi, S. Liu, Q. Guo, J. Zhang, S. Liang, M. He, and J. Luo. "Synthesis and characterization of amorphous MnO2/CNT via solid-state microwave for high-performance supercapacitors." International Journal of Energy Research 44 (2020) 4556-4567.

[15] X. Guo-Ting, C. Li, K. Wang, and L. W. Li. "Structural design and electrochemical performance of PANI/CNTs and MnO2/CNTs supercapacitor." Science of Advanced Materials 11 (2019) 1079-1086.

[16] W. Hongjuan, C. Peng, F. Peng, H. Yu, and J. Yang. "Facile synthesis of MnO2/CNT nanocomposite and its electrochemical performance for supercapacitors." Materials Science and Engineering: B 176 (2011) 1073-1078.

[17] Li. Gao-Ren, Z. P. Feng, Y. N. Ou, D. Wu, R. Fu, and Y. X. Tong. "Mesoporous MnO2/carbon aerogel composites as promising electrode materials for high-performance supercapacitors." Langmuir 26 (2010) 2209-2213.

[18] J. G. Wang, Y. Yang, Z. H. Huang, and F. Kang. "Coaxial carbon nanofibers/MnO2 nanocomposites as freestanding electrodes for high-performance electrochemical capacitors." Electrochimica Acta 56 (2011) 9240-9247.

[19] P. Yiting, Z. Chen, J. Wen, Q. Xiao, D. Weng, S. He, H. Geng, and Y. Lu. "Hierarchical manganese oxide/carbon nanocomposites for supercapacitor electrodes." Nano Research 4 (2011) 216-225.

[20] S. Burhanuddin, A. Yarmo, and B. M. Yamin. "Synthesis and characterisation of manganese oxides from potassium permanganate and citric acid mixtures." In AIP Conference Proceedings American Institute of Physics 157 (2013) 1932-937.

[21] J. Christian M., and A. Mauger. "Nanostructured MnO2 as electrode materials for energy storage." Nanomaterials 7 (2017) 396.

[22] A. Hashem, H. Abuzeid, M. Kaus, S. Indris, H. Ehrenberg, A. Mauger, C. M. Julien, "Green synthesis of nanosized manganese dioxide as positive electrode for lithium-ion

batteries using lemon juice and citrus peel." Electrochimica Acta 262 (2018) 74-81.
[23] P. Yola Prihardini Sasqia, and A. Awaluddin. "Manganese Oxide Synthesis of Birnessite Type Using Sol-Gel Method for Methylene Blue Degradation." In International Conference of CELSciTech 2019-Science and Technology track (ICCELST-ST 2019) 75-79.
[24] S. M. Benoy, M. Pandey, D. Bhattacharjya, and B. K. Saikia. "Recent trends in supercapacitor-battery hybrid energy storage devices based on carbon materials." Journal of Energy Storage 52 (2022) 104938.
[25] S. Surjit, P. Pazhamalai, V. K. Mariappan, G. K. Veerasubramani, N. Kim, and Sang-Jae Kim. "Hydrothermally synthesized chalcopyrite platelets as an electrode material for symmetric supercapacitors." Inorganic Chemistry Frontiers 7 (2020) 1492-1502.
[26] S. Yuanlong, M. F. El-Kady, J. Sun, Y. Li, Q. Zhang, M. Zhu, H. Wang, B. Dunn, and R. B. Kaner. "Design and mechanisms of asymmetric supercapacitors." Chemical reviews 118 (2018) 9233-9280.
[27] Z. Man, A. Bahi, Y. Zhao, L. Lin, F. Ko, P. Servati, S. Soltanian et al. "Enhancement of charge transport in interconnected lignin-derived carbon fibrous network for flexible battery-supercapacitor hybrid device." Chemical Engineering Journal 409 (2021) 128214.
[28] G. Dong-Cai, S. Tian, Y. Hui Sun, F. Deng, J. Min Nan, G. Zheng Ma, and Y. P. Cai. "Investigation of the electrochemical properties and kinetics of a novel SnFe2O4@ nitrogen-doped carbon composite anode for lithium-ion batteries." Electrochimica Acta 322 (2019) 134722.
[29] S. Shin, J. Jang, S. H. Yoon, and I. Mochida. "A study on the effect of heat treatment on functional groups of pitch based activated carbon fiber using FTIR." Carbon 35 (1997) 1739-1743.
[30] H. Saadia, N. Iqbal, T. Noor, N. Zaman, and K. Vignarooban. "Electrocatalytic study of NiO-MOF with activated carbon composites for methanol oxidation reaction." Scientific Reports 11 (2021) 17192.
[31] F. Rauf, S. J. Peighambardoust, S. H. Peighambardoust, M. Pateiro, and J. M. Lorenzo. "Adsorption of crystal violet dye using activated carbon of lemon wood and activated carbon/Fe3O4 magnetic nanocomposite from aqueous solutions: a kinetic, equilibrium and thermodynamic study." Molecules 26 (2021) 2241.
[32] Y. Zhang, H. Wei, H. Kimura, D. Wu, X. Xie, X. Yang, C. Hou, X. Sun, and W. Du. "Facile synthesis, microstructure and electrochemical performance of peanut shell derived porous activated carbon /Co3O4 composite for hybrid supercapacitors." Ceramics International 48 (2022) 34576-34583.